Contents lists available at ScienceDirect

Palaeogeography, Palaeoclimatology, Palaeoecology

Geologic variability of conodont strontium isotopic composition quantified by laser ablation multiple collection inductively coupled plasma mass spectrometry

Julie M. Griffin [a,b,*], Isabel P. Montañez [b], Justin J.G. Glessner [c], Jitao Chen [b,d], Malte Willmes [e,f]

[a] Department of Geology, California State University -Sacramento, 6000 J Street, Sacramento, CA 95819, USA
[b] Department of Earth and Planetary Sciences, University of California - Davis, One Shields Avenue, Davis, CA 95616, USA
[c] Interdisciplinary Center for Plasma Mass Spectrometry, University of California - Davis, One Shields Avenue, Davis, CA 95616, USA
[d] State Key Laboratory of Palaeobiology and Stratigraphy, Nanjing Institute of Geology and Palaeontology and Center for Excellence in Life and Paleoenvironment, Chinese Academy of Sciences, Nanjing 210008, China
[e] Institute of Marine Sciences, University of California - Santa Cruz, 115 McAllister Way, Santa Cruz, CA 95064, USA
[f] National marine Fisheries Service, Southwest Fisheries Science Center, 110 McAllister Way, Santa Cruz, CA 95064, USA

ARTICLE INFO

ABSTRACT

Conodont microfossils record seawater strontium isotope values (^{87}Sr/^{86}Sr), permitting chemostratigraphic correlation for tectonic and climatic reconstructions of the Paleozoic and early Mesozoic (541–201 Ma). Laser ablation multiple collection inductively coupled plasma mass spectrometry (LA MC-ICP-MS) can provide rapid, high spatial resolution ^{87}Sr/^{86}Sr analysis of conodont bioapatite but has not been validated by comparison with solution analysis. Validation of LA MC-ICP-MS should be completed in order to use the conodont ^{87}Sr/^{86}Sr values for age-correlations and environmental interpretations. Here, for the first time, we compare solution and LA MC-ICP-MS ^{87}Sr/^{86}Sr analyses of Carboniferous-age conodonts. Furthermore, we use quadrupole LA ICP-MS to determine concentrations of trace elements potentially responsible for isobaric interferences. Using increased mass resolving power ($m/\Delta m = {\sim}7500$) and analyzing conodont tissue with low ^{85}Rb/^{88}Sr (< 0.001), we find laser ablation copacetic with solution ^{87}Sr/^{86}Sr values. The two-standard-deviation of these LA ^{87}Sr/^{86}Sr ratios (average 2SD = 0.00105) are within the two-standard-error uncertainty of solution measurements (average 2SE = 0.00001) on conodonts from the same stratigraphic level. The LA measurements are at a higher spatial resolution and on average 0.00015 higher than solution measurements. Uncertainty of the mean calculations, made on duplicate LA MC-ICP-MS analyses of individual conodonts from the same stratigraphic level, exhibit ^{87}Sr/^{86}Sr variability beyond the precision of reference materials (2SE = 0.00001). This finding suggests that solution ^{87}Sr/^{86}Sr values determined by dissolving multiple conodonts are homogenizing the conodont ^{87}Sr/^{86}Sr signal. As such, the precision of these solution measurements does not capture the geologic variability of conodont ^{87}Sr/^{86}Sr within a stratigraphic level, which may originate from differential diagenetic alteration. Conodont ^{87}Sr/^{86}Sr measurements that do not account for this variability are at risk of false calibrations with the paleo-seawater ^{87}Sr/^{86}Sr curve, which has implications for the timing of geologic events and reconstructions of paleo-environmental changes.

1. Introduction

Studies of palaeoceanography and palaeoclimatology utilize the strontium isotope ratio (^{87}Sr/^{86}Sr) of fossils and sediments to reconstruct the ^{87}Sr/^{86}Sr of seawater, which in turn constrains changes in continental weathering, tectonic activity, and climate (Raymo and Ruddiman, 1992; Montañez et al., 1996, 2000; Jones and Jenkyns, 2001; Banner, 2004; Prokoph et al., 2008; Reyes et al., 2014; Van Der Meer et al., 2014; Chen et al., 2018). The common occurrences of conodonts, apatite microfossil remains of a nektonic organism (Sweet and Donoghue, 2001), in marine deposits permits the construction of high resolution ^{87}Sr/^{86}Sr isotope timeseries in Paleozoic and early Mesozoic

---

sediments (Ruppel et al., 1996; John et al., 2008; Brand et al., 2009; Woodard et al., 2013; Saltzman et al., 2014; Montañez et al., 2018). Fossil bioapatite such as conodonts incorporates elements like Sr both in vivo and during post-mortem stabilization and precipitation of authigenic apatite (i.e., recrystallization; Tuross et al., 1989; Kolodny et al., 1996; Trueman and Tuross, 2002; Berna et al., 2004; Tütken et al., 2008; Herwartz et al., 2013; Keenan et al., 2015; Keenan and Engel, 2017). Chemostratigraphic records from conodont bioapatite are particularly useful for successions in which biogenic calcites are less common or irregularly distributed (Brand and Bruckschen, 2002). Furthermore, studies suggest conodont bioapatite to be diagenetically more robust than contemporaneous biogenic carbonates (Wenzel et al., 2000; Barham et al., 2012). Constructions of conodont-based $^{87}Sr/^{86}Sr$ records, however, lag behind other contemporaneous isotope records (i.e., $\delta^{18}O$, $\delta^{13}C$) partly because the traditional $^{87}Sr/^{86}Sr$ analysis method is time and labor intensive, especially when considering the micro-drilling and selective chromatography needed to purify strontium from dissolved material. Given that laser ablation (LA) yields accurate and precise values for carbonates (Christensen et al., 1995; Woodhead et al., 2005; Wortham et al., 2017), and igenous aptatite crystals (Bizzarro et al., 2003; Yang et al., 2009; Munoz et al., 2016), LA is a promising technique for rapid $^{87}Sr/^{86}Sr$ analyses of conodont bioapatite. The LA technique needs to be validated for conodont bioapatite prior to application to geologic questions because recent LA analyses of modern and Cenozoic bioapatites yield non-systematically elevated and less precise $^{87}Sr/^{86}Sr$ values relative to solution analyses (LA RSD = 0.04–0.15%, solution RSD = 0.001–0.006%; Horstwood et al., 2008; Simonetti et al., 2008; Irrgeher et al., 2016). While conodont bioapatite is similar to the teeth and bones analyzed in these studies, the structure is somewhat unique (Trotter et al., 2007). Conodont apatite has also undergone several million more years of diagenesis. The LA technique needs to be validated for determining conodont bioapatite $^{87}Sr/^{86}Sr$ prior to application to geologic questions.

The first published study (Song et al., 2015) of LA multi-collector inductively coupled plasma mass spectrometry (MC-ICP-MS) for $^{87}Sr/^{86}Sr$ analysis of Permian-Triassic boundary conodonts published values but lacked adequate reference materials for duplication, as well as a comparison to solution to assess the accuracy of the LA approach. Further, the analytical precision of the unknown conodont $^{87}Sr/^{86}Sr$ values was not reported. Offset and non-systematic elevation of $^{87}Sr/^{86}Sr$ values measured by LA in recent and Cenozoic bioapatite is partially due to $^{40}Ca^{31}P^{16}O^+/^{40}Ar^{31}P^{16}O^+$ formed by the ablation of the apatite matrix in combination with the carrier gases (Ar), which creates an artificial signal on mass 87 (Horstwood et al., 2008; Vroon et al., 2008; Lewis et al., 2014; Willmes et al., 2016a&b; Irrgeher et al., 2016; see contrasting arguments in Copeland et al., 2008; Müller and Anczkiewicz, 2016). Additionally, trace elements within fossil bioapatite generate spectral interferences on the masses of Sr, Rb, and Kr (Table 1) (Horstwood et al., 2008; Vroon et al., 2008; Lewis et al., 2014; Willmes et al., 2016a; Irrgeher et al., 2016). Interferences on the masses of Sr create artificial values for ^{87}Sr, ^{86}Sr, and the mass bias correction

(Bizzarro et al., 2003), while additional signal on the masses 85 (^{85}Rb) and 83 (^{83}Kr) causes over correction for the spectral interferences of ^{87}Rb and ^{84}Kr on ^{87}Sr and ^{84}Sr, respectively (Ramos et al., 2004; Zhang et al., 2018). Therefore, analyses of conodont $^{87}Sr/^{86}Sr$ by LA MC-ICP-MS need to consider the influence of these trace elements in the analysis protocol and data evaluation. In contrast, $CaPO^+$ ions and trace elements do not impact solution-based $^{87}Sr/^{86}Sr$ analysis as the interfering ions are removed through cation-exchange column chemistry before the MC-ICP-MS analysis.

If LA MC-ICP-MS yields accurate and precise conodont $^{87}Sr/^{86}Sr$ values, then this approach would greatly increase the potential for integrating $^{87}Sr/^{86}Sr$ into deep-time studies. The minor amount of bioapatite required for LA MC-ICP-MS relative to solution analysis (~150 μg, equivalent to one to dozens of conodont elements) makes $^{87}Sr/^{86}Sr$ measurements possible for sample sets with a low abundance of conodonts. LA MC-ICP-MS also permits evaluation of $^{87}Sr/^{86}Sr$ variability between individual conodonts, which cannot be detected due to the homogenization of multiple conodonts (n = 3–50) required to accumulate enough material for solution $^{87}Sr/^{86}Sr$ analysis.

Here we evaluate the accuracy and precision of LA MC-ICP-MS for conodont $^{87}Sr/^{86}Sr$ analysis through a comparison of $^{87}Sr/^{86}Sr$ values measured by solution and LA MC-ICP-MS analyses. The conodonts analyzed were extracted from Carboniferous-age deposits in the U.S.A., China, and Ukraine. We further quantify the presence of multiple isobaric interferences on the masses of strontium and other elements that need to be corrected for accurate $^{87}Sr/^{86}Sr$ measurements. We demonstrate a mass filtering technique for reducing these interferences. We use this in situ technique to identify the magnitude of $^{87}Sr/^{86}Sr$ variability between individual conodonts extracted from the same stratigraphic level and quantify how this population-scale variability influences age-reconstructions based on conodont $^{87}Sr/^{86}Sr$ chemostratigraphy.

2. Experimental protocol

2.1. Conodont preparation and treatment

Conodonts from 23 individual stratigraphic intervals of limestone and shale were split into two or more aliquots for $^{87}Sr/^{86}Sr$ analysis by solution and laser ablation MC-ICP-MS. Every laser ablation and solution analysis of conodont(s) from one stratigraphic level is a considered a duplicate. True replicates cannot be obtained by laser ablation because it is impossible to ablate the same exact material twice, except in cases of absolute spatial homogeneity. The conodonts span a range of conodont alteration indices (CAI; Epstein et al., 1977) and were extracted from a variety of lithologies representing different depositional environments (Table 2). Conodonts were physically cleaned, screened, and leached prior to both LA and solution $^{87}Sr/^{86}Sr$ analysis. All samples were sonicated in deionized water (18 MΩcm^{-1}) for ~20 s to remove adhering material (Ebneth et al., 1997). Following sonication, selected samples were imaged using a Hitachi TM 3000 tabletop environmental scanning

Table 1
Atomic mass units of the elements and molecules that create isobaric interferences on the masses of Sr and related elements required for accurate and precise $^{87}Sr/^{86}Sr$ measurement (modified from Vroon et al., 2008). "Detector" row provides the detector array utilized on the Nu Plasma HR (Nu032) MC-ICP-MS for strontium isotope analyses. Most abundant isotopes of that element or molecule italicized.

	89	88.5	88	87.5	87	86.5	86	85.5	85	84	83.5	83	82	80
Detector			H4		H2	H1	Ax	L1	L2	L3	IC1	L4		
Sr^+			*87.9056*		86.9089		85.9093			83.9134				
Rb^+					*86.9092*				84.9118					
Kr^+							85.9106			*83.9115*		82.9141	81.9135	79.9164
$CaPO^+$	88.9355		87.9355		*86.9313*									
$ArPO^+$					86.9311				84.9314			82.9362		
Er^{2+}									84.9677	83.9662	83.4660	*82.9652*	81.9646	
Yb^{2+}			87.9713		86.9694	86.4691	*85.9682*	85.4682	84.9674	83.9670				
FeP^+	88.9070		87.9092		*86.9087*				84.9134					

Table 2
Characteristics of analyzed conodont samples.

Locality	Latitude & Longitude	Age (ICC[a] Stages)	Lithology[b]	CAI[c]
Kansas City, MO, USA	N39°00′44″, W94°29′58″	Kasimovian (307–303 Ma)	black shale; carbonate p/g, w/p, shale	1
Black Hills, SD, USA	N43°58′46″, W103°44′57″	Moscovian (315–307 Ma)	green shale	1
Moapa, NV, USA	N36°43′50″, W114°46′19″	Miss-Penn boundary (323 Ma), Moscovian (315–307 Ma)	carbonate p/g	2
Bezim'yane, Ukraine	N48°35′43″, E37°40′51″	Serpukhovian (330–323 Ma), Miss-Penn Boundary (323 Ma)	carbonate	5
Horlivka, Ukraine	N48°18′29″, E38°01′53″	Moscovian (315–307 Ma)	carbonate	4
Kalynove, Ukraine	N48°08′24″, E37°26′32″	Kasimovian (307–303 Ma)	carbonate p/g	3
Naqing, South China	N25°14′40″, E106°29′26″	Visean (346–330 Ma), Serpukhovian (330–323 Ma)	carbonate p/g, w/p, mudstone	5

[a] ICS = International Chronostratigraphic Chart (Cohen et al., 2013).
[b] p/g = packstone/grainstone; w/p = wackestone/packstone.
[c] CAI = Conodont Alteration Index (Epstein et al., 1977).

electron microscope (eSEM), located at the University of California - Davis (UC Davis), to identify conodont elements with apatite overgrowths or recrystallization (Fig. 1) that may influence $^{87}Sr/^{86}Sr$ values (Barham et al., 2012). Where possible, conodonts lacking diagenetic features were used for analyses, but in some samples all the conodont elements exhibited overgrowths and thus had to be analyzed (Arrow Canyon, NV, USA; Naqing, *S. China*). All samples were further pretreated by leaching in 0.5% Optima™ acetic acid for ~14 h to remove the altered margins of conodonts (Ruppel et al., 1996). Although leaching is a common practice for conodont $^{87}Sr/^{86}Sr$ analysis, studies document

that the difference between the $^{87}Sr/^{86}Sr$ of the leachate and the leached elements is less than the precision of the analyses (John et al., 2008; Saltzman et al., 2014) and as such leaching may not improve the accuracy of results. Conodont tissues were identified as albid or hyaline prior to analysis by visual inspection of colour under a binocular microscope (Fig. 1), guided by previously described classifications (Trotter et al., 2007).

2.2. Solution MC-ICP-MS $^{87}Sr/^{86}Sr$ analyses

Pretreated conodonts for solution-mode $^{87}Sr/^{86}Sr$ analysis were weighed into aliquots of an average size of 146 μg, dissolved in 3 M Optima™ nitric acid, and then purified using 30 μL cation exchange columns (1 mL pipette tips), Eichrom Sr resin (100–500 μm), and a peristaltic pump. Analysis was carried out on a Nu Plasma HR (Nu032) multiple collection high-resolution double-focusing ICP-MS system housed in the Interdisciplinary Center for Plasma Mass Spectrometry at

Table 3
Instrument parameters for $^{87}Sr/^{86}Sr$ analysis.

Nu Plasma HR (Nu032) MC-ICP-MS	
RF power	1300 W
Analyser pressure	$<2.8 \times 10^{-8}$ mbar
Cones	high-sensitivity sampler, standard skimmer (both nickel)
Gas flows	
Coolant (Ar)	13.0 L/min
Auxiliary Gas (Ar)	0.85 L/min
Mix Gas 1 (Ar)	1.15 L/min
Laser ablation system	
New Wave Research UP213 Nd:YAG 213 nm laser	
Laser fluence	7–10 J/cm²
Repetition rate	10 Hz
Spot size	Exp 1: 40–65 μm circle
	Exp 2: 65–100 μm wide, ~300 μm long line
He gas from cell	0.7 L/min

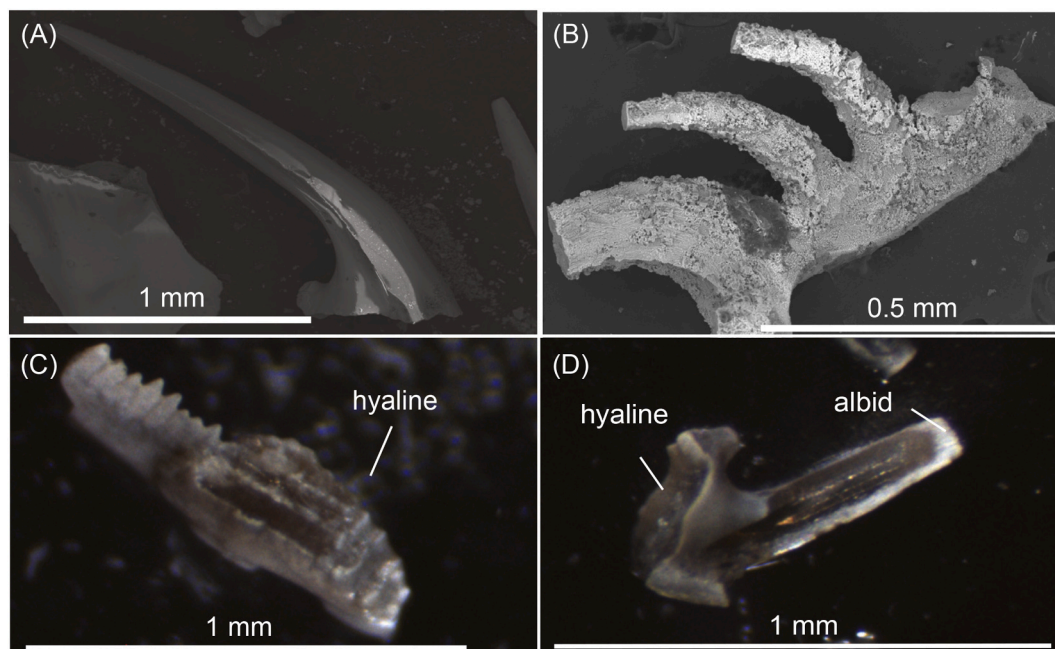**Fig. 1.** Images of conodonts analyzed for $^{87}Sr/^{86}Sr$. Environmental Scanning Electron Microscope (eSEM) images of (A) *Idioprioniodus* P element from the Moscovian of the Black Hills, South Dakota, USA and (B) Unknown genera S element from the Visean-Serpukhovian of South China. Conodonts reveal a lack of mineralization (A) and extensive remineralization (B). Binocular microscope images of (C) *Idiognathodus* P element from the Kasimovian of Kansas City, MO, USA, and (D) *Idioprioniodus* P element from the Kasimovian of Kansas City, MO, USA. Conodonts labeled to indicate hyaline tissue (C) as well as albid tissue (D) identified by colour and translucency of material.

UC Davis (Table 3). Solutions were diluted to ~1 ppb running concentrations and introduced through a DSN-100 desolvating nebulizer into the mass spectrometer. The 1 ppb concentration was chosen because this solution generates 1–2 V of total Sr signal, which is equivalent to the signal generated by laser ablation of conodonts. Sample-standard bracketing and linear correction methods were used to normalize sample values to a NIST SRM 987 value of 0.710249 (GeoReM database, Jochum et al., 2005). Separate NIST SRM 987 solutions, also at 1 ppb, were analyzed as an unknown and yielded an average value of 0.710251 ± 0.000026 (2σ, *n* = 44).

2.3. Laser ablation MC-ICP-MS $^{87}Sr/^{86}Sr$ analyses

For over a decade, laser ablation studies of apatite minerals have argued that multiple interferences influence $^{87}Sr/^{86}Sr$ values and have presented a variety analytical and correction techniques. The CaPO$^+$ and ArPO$^+$ molecular interferences are hypothesized to increase signal on mass 87 and thus increase $^{87}Sr/^{86}Sr$ values (Simonetti et al., 2008; Horstwood et al., 2008; Willmes et al., 2016 a&b) but have not been consistently identified in solution or LA analyses (Copeland et al., 2008; Müller and Anczkiewicz, 2016). Although previous studies have hypothesized a CaPO$^+$ interference, it cannot be differentiated from the ArPO$^+$ interference because of the lack of a Ca-free phosphate solid. CaPO$^+$/ArPO$^+$ polyatomic interferences have not been consistently identified with solution sample introduction (Müller and Anczkiewicz, 2016), perhaps because in solution these elements exist as calcium and phosphate ions separated through hydrolysis. Calcium/Argon and phosphorus would need to synthesize in the ICP plasma to form the CaPO$^+$/ArPO$^+$ species. Conversely, LA sample introduction directly injects aerosol condensed calcium-phosphate particles into the ICP plasma and hence may more easily create CaPO$^+$ molecules sampled into the mass spectrometer.

We used an ion counter and magnet scans to monitor signals for a range of masses at the high end of the ^{87}Sr peak with the Nu Plasma HR MC-ICP-MS configured to an enhanced mass resolving power (R_{power} = ~7500). Ablation of a marine biogenic calcium carbonate, an in-house White Seabass (*Atractoscion nobilis*) otolith (SBO) reference material, did not produce an anomalous signal on the high mass side of ^{87}Sr (Fig. 2A). Conversely, ablation of a piece of the igneous Durango apatite with the torch normally positioned did produce a secondary peak, or "shoulder," on the high mass side of the ^{87}Sr peak (Fig. 2B). This shoulder is likely due to a signal peak that is offset but overlaps the ^{87}Sr peak and that is generated by $^{40}Ca^{31}P^{16}O^+$ and/or $^{40}Ar^{31}P^{16}O^+$ (Table 1, Willmes et al., 2016b). The lack of a similar shoulder on the high mass side of the ^{87}Sr peak during calcium carbonate ablation indicates this is a spectral interference on mass 87 in apatite that will impact the measured $^{87}Sr/^{86}Sr$ value. Previous authors (Willmes et al., 2016b) suggested that increasing the plasma sampling depth minimizes this interfering peak, as backing out the torch decreased $^{88}Sr^{16}O/^{88}Sr$ values (proxy for $^{40}Ca^{31}P^{16}O^+/^{40}Ar^{31}P^{16}O^+$) measured on modern bioapatites. By increasing the residence time in the plasma (i.e., increasing the plasma sampling depth) more of the CaPO$^+$ species are broken apart. We document the effectiveness of this technique by showing a minimization of the $^{40}Ca^{31}P^{16}O^+/^{40}Ar^{31}P^{16}O^+$ spectral interference on mass 87 by moving the torch at a greater distance from the cone (compare Fig. 2B and C). In response to this replication of previous findings (Irrgeher et al., 2016), we tested two different techniques for $^{87}Sr/^{86}Sr$ analysis of conodont apatite that minimize spectral interferences.

The two LA MC-ICP-MS experiments for $^{87}Sr/^{86}Sr$ analysis of conodont apatite used two different inductively coupled plasma sampling depths and mass resolving powers. Increasing the distance between the torch and the sampling cone increases the plasma sampling depth and reduces the occurrence of molecular interferences that generate invalid signals on the masses of interest (Benson et al., 2013; Willmes et al., 2016 a&b; Sellheim et al., 2017). Unrelated to torch position, the mass resolving power of the MC-ICP-MS determines the degree of
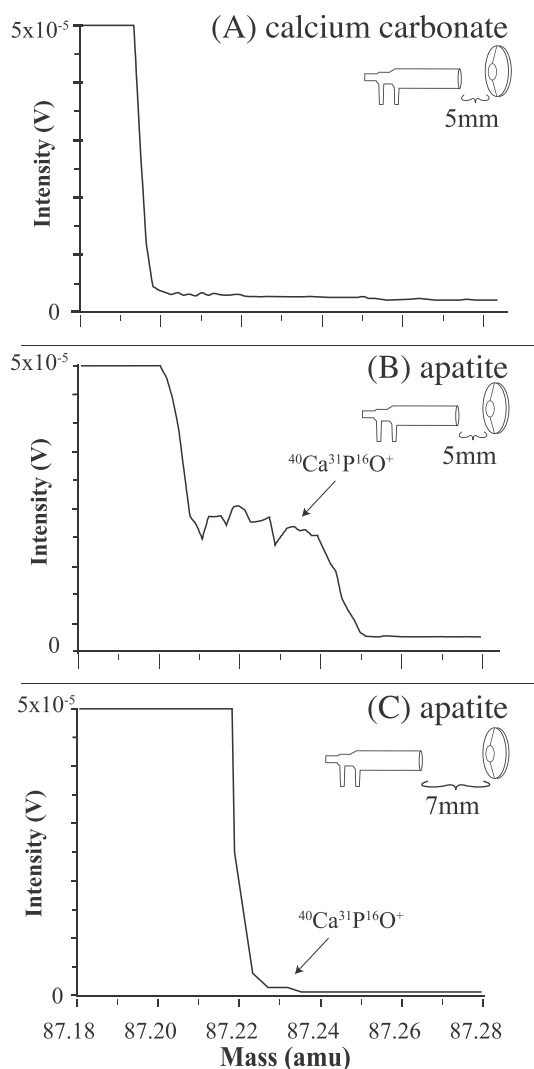

Fig. 2. Results of magnet scans. Magnet scans of high side of mass 87 peak with MC-ICP-MS tune to medium mass resolving power ($m/\Delta m$ = ~7500). LA of (A) calcium carbonate with the torch in normal position ("in"), (B) apatite with the torch in, and (C) backed out. The presence of the $^{40}Ca^{31}P^{16}O^+$ molecule during LA of apatite is apparent (compare A and B) and reduced by increasing the sampling distance of the torch (compare B and C).

discrimination between atomic masses and enables separation of spectral interferences (Wieser et al., 2012). Resolving power (R_{power}) is defined by:

$$R_{power} = \frac{m_i}{m_2 - m_1} \qquad (1)$$

In Eq. (1), m_i is the mass being measured by that signal peak as a whole number, m_1 is the mass where the signal peak initially exceeds background (5%), and m_2 is the mass at the initial full height (95%) of the signal peak. The same equation (Eq. (1)) is used to determine the mass resolution (R) required to distinguish between two offset and overlapping signal peaks. In this case, m_i is the mass/charge of interest as a whole number, while m_1 and m_2 are atomic mass units/charge of the spectral interferences. For example, determining the mass resolution required for separating $^{87}Sr^+$ (mass/charge = 86.90889/1 = 86.90889) from $^{174}Yb^{2+}$ (mass/charge = 173.93887/2 = 86.96944) while measuring mass 87 yields a R equal to 87/(86.96944–86.90889) or 1437. Therefore, the R_{power} determined by the peak shape (Eq. (1)) must be ≥1437. Increased resolving power is achieved by narrowing the source slit (set to 0.05 mm and with alfa slits engaged, each with 25%

signal reduction), which decreases overall Sr signal transmission by ~90%. Increased plasma sampling depth was also found to decrease the Sr signal transmission ~40%. Increasing the spot size of the laser was used to overcome these losses in Sr transmission.

As both increased resolving power and increased plasma sampling depth decrease signal transmission, two independent experiments testing the effectiveness of each technique were carried out. Experiment 1 utilized low mass resolving power (R_{power} = ~300) and an increased plasma sampling depth (6 to 7 mm on the UCD setup) to decrease the presence of $^{40}Ca^{31}P^{16}O^+$ and $^{40}Ar^{31}P^{16}O^+$ interferences (Willmes et al., 2016b). Experiment 2 utilized a more commonly applied plasma sampling depth (4.5 to 5.5 mm) and medium mass resolving power (R_{power} = ~7500) to attenuate spectral interferences.

Conodonts for LA were mounted on double stick tape. The small and delicate nature of conodonts leads to substantial loss (up to 50% of a set) during the process of epoxy mounting and polishing to a flat surface. LA MC-ICP-MS analysis of curved bioapatite surfaces has been demonstrated to not alter measured $^{87}Sr/^{86}Sr$ ratios (Le Roux et al., 2014). Conodonts were ablated by a solid state UP213 Nd:YAG 213 nm laser (New Wave Research) interfaced with a SuperCell laminar flow chamber using He carrier gas, to the same Nu Plasma HR MC-ICP-MS that analyzed solution samples (Table 3). In Experiment 1, reported $^{87}Sr/^{86}Sr$ values for individual conodonts are the average of three 65 μm diameter spots. In Experiment 2, $^{87}Sr/^{86}Sr$ values were determined by ablating a line ~300 μm long and 65 μm wide across each conodont at a traverse rate of approximately ≤5 μm/s. Given the μm-scale size of individual conodonts, none could be analyzed by both experiments, so instead multiple conodonts from five individual stratigraphic intervals were analyzed by both experiments. Lines were used for Experiment 2 because this resulted in more material entering the machine to overcome the decreased sample transmission (sensitivity) associated with increased mass resolving power. Increasing the mass resolving power and decreasing the plasma sampling depth from Experiment 1 to 2 resulted in a 42% decrease in sample transmission (Table 4). Specifically, the average total Sr signal measured for an in-house bioapatite standard (Sterling Sturgeon Fin Ray) decreased from 1.2 V in Experiment 1 to 0.7 V in Experiment 2. The change in ablation style and sample transmission, however, did not influence the measured $^{87}Sr/^{86}Sr$ as the values for two in-house marine bioapatite standards measured in each experiment are within error (Table 4). Laser fluency, as measured by the New Wave laser software, was between 7 and 10 J/cm² with the laser set to a 10 Hz (pulses per second) rate (Table 3).

LA MC-ICP-MS data was reduced using the R (R Core Team, 2020) script IsoFishR (Willmes et al., 2019). Background values, determined in the first 30 s of analysis prior to laser firing, were subtracted from the time series data (averages: 0.005 V on mass 84, 0.05 V on mass 86) to remove Kr interferences (Table 1). An exponential mass bias correction factor for each data point in the time series was subsequently calculated by normalizing the $^{86}Sr/^{88}Sr$ value to 0.1194 (GeoReM database, Jochum et al., 2005). Rb interference was corrected for by using the strontium mass bias factor and ^{85}Rb signal to calculate the ^{87}Rb signal and subtract it from the mass 87 signal, leaving ^{87}Sr. The mass bias factor was further applied to the $^{87}Sr/^{86}Sr$ ratio of each data point collected and integrated. A four-point moving average was applied to reduce the noise typically associated with LA data. A data time window, visualized as a peak in the Sr signal above background measurements, was selected and the average of all the $^{87}Sr/^{86}Sr$ ratios within that window was taken as the $^{87}Sr/^{86}Sr$ ratio of that conodont. Standard error about the mean is used to report the precision of individual $^{87}Sr/^{86}Sr$ analyses given that over 300 and 100 measurements were made for LA and solution analyses, respectively. Noise in the data is inherent to MC-ICP-MS and thus the spread of variability in this noise, indicated by the standard deviation, is not appropriate for evaluating the accuracy of measured values. Values with a weak mean total Sr signal (<0.5 V) for the integrated window were removed from the data set.

Given the lack of universally accepted certified isotopic reference

Table 4

Long-term precision for isotopic reference materials for LA MC-ICP-MS analysis. Voltage is a semi-quantitative indicator of the strontium concentration in material.

Reference material	$^{87}Sr/^{86}Sr$	^{88}Sr [V]	±2σ	±2se	n	Reference
Sea Bass Otolith	0.709178	2.6	0.000174	0.000013	45	Willmes et al., 2016a, 2016b; Sellheim et al., 2017
Green Sturgeon Fin Ray	0.709181	3.4	0.000211	0.000013	65	
Sterling Sturgeon Fin Ray	0.705620	1.6	0.000314	0.000020	62	
All						
Sea Bass Otolith	0.709098	3.0	0.000169	0.000015	23	This study
Green Sturgeon Fin Ray	0.709144	2.3	0.000113	0.000010	62	This study
Sterling Sturgeon Fin Ray	0.705698	0.9	0.000270	0.000022	37	This study
Durango	0.707749	1.9	0.000481	0.000051	9	This study
Experiment 1 - Low Resolution, Torch out						
Sea Bass Otolith	0.709099	3.0	0.000184	0.000017	20	This study
Green Sturgeon Fin Ray	0.709152	1.4	0.000132	0.000013	35	This study
Sterling Sturgeon Fin Ray	0.705626	1.2	0.000270	0.000030	17	This study
Experiment 2 - Medium Resolution, Torch in						
Sea Bass Otolith	0.709097	3.1	0.000401	0.000026	3	This study
Green Sturgeon Fin Ray	0.709134	1.4	0.000155	0.000012	27	This study
Sterling Sturgeon Fin Ray	0.705759	0.7	0.000443	0.000031	20	This study

materials (iRM) for bioapatites, we used one calcium carbonate and two bioapatite in-house reference materials to evaluate the analytical reproducibility of our LA MC-ICP-MS data. The following $^{87}Sr/^{86}Sr$ values are the average of both Experiment 1 and 2 analyses. The primary in-house iRM, a marine calcium carbonate White Seabass Otolith (SBO) from *Atractoscion nobilis*, yielded an average value of 0.709098 ± 0.000169 (2σ, n = 23) and mean ^{88}Sr signal of 3.0 V. The calcium carbonate SBO iRM ensures accurate and precise measurements of $^{87}Sr/^{86}Sr$ ratios without any of the spectral interferences inherent in bioapatite. Another in-house iRM, the marine bioapatite Green Sturgeon pectoral Fin Ray (GSFR) from *Acipenser medirostris*, yielded an average value of 0.709144 ± 0.000113 (2σ, n = 62) and mean ^{88}Sr signal of 2.3 V. A second bioapatite iRM, a freshwater Sturgeon pectoral Fin Ray (SSFR) from *Acipenser transmotanus,* with a lower Sr concentration (mean ^{88}Sr signal of 0.9 V), yielded an average value of 0.705698 ± 0.000270 (2σ, n = 37). The bioapatite iRMs are modern materials that have not been subjected to post-mortem diagenesis. $^{87}Sr/^{86}Sr$ values for both the GSFR and SSFR iRMs measured in Experiment 1 (low resolution, torch out) and Experiment 2 (medium resolution, torch in) are within error of each other (Table 4). The means and standard deviations of the three in-house iRMs compare well to values previously produced in this laboratory (Willmes et al., 2016b; Sellheim et al., 2017), indicating that the LA MC-ICP-MS analyses presented in this study are reliable (Table 4). The SBO and GSFR values match well with the modern ocean $^{87}Sr/^{86}Sr$, demonstrating the potential of modern marine materials to be used as comparable reference materials in other labs.

2.4. LA quadrupole ICP-MS analyses

The spectral interference of ^{87}Rb and doubly charged REEs has previously been evaluated in apatite (Bizzarro et al., 2003; Ramos et al., 2004; Horstwood et al., 2008; Copeland et al., 2008; Yang et al., 2014; Zhang et al., 2018), but not conodonts. Previous work (Ramos et al., 2004; Yang et al., 2009) measured masses 83.5 and 86.5 as proxies for ^{167}Er^{2+} and ^{173}Yb^{2+} respectively during Sr isotope measurements on a MC-ICP-MS. These voltages were scaled to different isotopes using natural abundances, and then subtracted from the signal on which the doubly charged REE isotope interfered (Table 1). We attempted to measure masses 83.5 and 86.5 using ion counters, but the signal was undetectable likely due to the low ratios of Yb/Sr and Er/Se (see Section 3.2) in comparison to the ratios in igneous apatite crystals (0.08) that influence strontium isotope measurements (Ramos et al., 2004). In order to accurately quantify the influence of these isobaric interferences, a selection of conodonts was further analyzed for elemental concentrations (Fe, Yb, Er, Sr) using a Photon Machines 193 nm ArF Eximer laser with a HelEx dual-volume LA cell coupled to an Agilent 7700× quadrupole ICP-MS currently housed at the Interdisciplinary Center for Plasma Mass Spectrometry at UC Davis (Table 5). Square spots, 45 μm per side were ablated at a repetition rate of 10 Hz. Laser fluence was typically 3 J/cm^2. Trace element concentration values were determined by averaging the data for two to five spots made on an individual conodont element. Conodont bioapatite was assumed to contain 37.8 wt% Ca (Trotter and Eggins, 2006). Data were reduced relative to values of NIST SRM 610 analyzed as a reference material using Iolite v4.2.1 "Trace Elements" data reduction scheme (Woodhead et al., 2007; Patton et al., 2011). The internal standard was ^{43}Ca. Separate ablations of NIST SRM 610 glass were also reduced to confirm the effectiveness of data reduction. The averages of ^{166}Er/^{88}Sr, ^{174}Yb/^{88}Sr, and ^{57}Fe/^{88}Sr analyses of NIST SRM 610 reduced as an unknown are within error of published values (Table 6).

2.5. Statistical analyses

The results of these analyses were compared using paired *t*-tests (Table 7) and correlation tests (Table 8) facilitated by the statistics package of Octave (Eaton et al., 2018). Whether the data sets compared were normally distributed or not was evaluated on the basis of skewness and kurtosis using a code modified for Octave (Trauth, 2010). The data set from Experiment 1 is normally distributed ($n = 40$). The skewness for Experiment 2 is positive, and the kurtosis is high. However, the dataset contains 73 pairs (n) and thus can be treated as a normal distribution. While the trace element datasets (Er/Sr, Yb/Sr, Fe/Sr, Rb/Sr) all exhibited a skew towards lower values than the mean, the number of Fe/Sr and Rb/Sr analyses were sufficient to be considered a normal distribution ($n = 35$ and $n = 113$, respectively). The Er/Sr and Yb/Sr datasets fall short of the number of analyses sufficient to be considered a normal

Table 5
Instrument parameters for trace element analysis.

Agilent 7770× Quadrupole ICP-MS	
RF power	1350 W
Analyser pressure	$<1.3 \times 10^{-6}$ mbar
Dwell time per mass	60–300 ms (varied)
Total sweep time	900 ms (varied)
Gas flows	
Coolant Gas (Ar)	15 L/min
Auxiliary Gas (Ar)	1.0 L/min
Carrier Gas (Ar)	1.0 L/min (tuned daily)
Photon Machines 193 nm ArF Eximer Laser System with HelEx dual-volume cell	
Laser Fluence	~3.0 J/cm^2
Repetition Rate	10 Hz
Spot Size	45 μm
He gas from cell	1.0 L/min

Table 6
Accuracy and precision of LA ICP-MS analysis from running NIST SRM 610 as an unknown.

	^{166}Er/^{88}Sr	^{173}Yb/^{88}Sr	^{57}Fe/^{88}Sr
Jochum et al., 2011	*0.883*	*0.873*	*0.888*
Average	0.884	0.873	0.886
2SD[a]	0.025	0.026	0.042
% RSD[b]	2.82	2.92	4.72
n	34	34	18

[a] SD = standard deviation.
[b] RSD = relative standard deviation.

Table 7
Results of hypothesis testing at the 5% confidence interval. HO is null hypothesis, HA is alternative hypothesis.

Hypotheses	Dataset Names (n)	Result, P-values
HO: LA ratios = solution ratios HA: LA ratios ≠ solution ratios	Exp 1 ($n = 40$) Exp 2 ($n = 73$)	Exp 1: HA, 6.0×10^{-13} Exp 2: HA, 4.5×10^{-12}
HO: Δ ^{87}Sr/^{86}Sr Exp 1 ≤ Δ ^{87}Sr/^{86}Sr Exp 2 HA: Δ ^{87}Sr/^{86}Sr Exp 1 > Δ ^{87}Sr/^{86}Sr Exp 2	Exp 1 (n = 40) Exp 2 (n = 73)	HA, 5.9×10^{-5}
HO: ^{87}Sr/^{86}Sr Exp 1 2SE ≤ ^{87}Sr/^{86}Sr Exp 2 2SE HA: ^{87}Sr/^{86}Sr Exp 1 2SE > ^{87}Sr/^{86}Sr Exp 2 2SE	Exp 1 2SE ($n =$ 40) Exp 2 2SE (n = 73)	HA, 2.2×10^{-8}
HO: Δ ^{87}Sr/^{86}Sr albid ≥ Δ ^{87}Sr/^{86}Sr hyaline (Exp 2) HA: Δ ^{87}Sr/^{86}Sr albid < Δ ^{87}Sr/^{86}Sr hyaline (Exp 2)	Albid ($n = 19$) Hyaline ($n =$ 36)	HO, 1.0 *(see text)*

Table 8
Results of Pearson correlation testing between trace element concentrations and the offset between laser and solution ^{87}Sr/^{86}Sr measurements. All bolded correlation coefficients are significant, as the probability of yielding a correlation coefficient as high with a set of random values is less than 5%. *P*-values (p) less than 0.05 indicate this significance.

	Correlation Coefficient	p	n
Rb/Sr	**0.28**	0.003	113
Er/Sr	0.37	0.09	21
Yb/Sr	0.12	0.59	21
Fe/Sr	0.27	0.11	35

distribution ($n = 21$ for both), and thus the results of the correlation tests must be considered preliminary. Intra-sample (stratigraphic level) variability was determined by calculating the uncertainty of the mean at a 95% confidence interval, which considers the values measured to be a subset of the infinite ^{87}Sr/^{86}Sr values possible one stratigraphic level (McArthur et al., 2001). The uncertainty of the mean assumes infinite analyses are possible for each stratigraphic level and that the values measured are just a sample of these infinite possibilities. The range provided by the uncertainty of the mean thus includes the true value for 95% of all the possible average ^{87}Sr/^{86}Sr values for a stratigraphic level and is determined by the following formula:

$$\pm t_{95,n-1}\left(\text{s.d.}/\sqrt{n}\right) \tag{2}$$

where t_{95} is the 95th percentile of the Student *t* distribution with (n-1) degrees of freedom, n is the number of samples, and s.d. is the standard deviation (McArthur et al., 2001).

3. Results

The results of this study demonstrate that LA MC-ICP-MS analysis for

^{87}Sr/^{86}Sr of conodont bioapatite measured within error of solution analyses from the same stratigraphic level. LA values are repeatedly elevated/heavy relative to solution values (Fig. 3), which has been documented in previous studies of tooth enamel and bone (Simonetti et al., 2008; Horstwood et al., 2008; Copeland et al., 2008; Lewis et al., 2014; Willmes et al., 2016a). The average of the two-standard-error (2SE) values from solution ^{87}Sr/^{86}Sr measurements is 0.000010 (n = 28), whereas that of LA measurements is eight times greater (0.000082; n = 113). In response to these findings, this study presents a new methodology to improve the LA precision and identify the source of the elevated ^{87}Sr/^{86}Sr ratios.

3.1. Solution versus LA ^{87}Sr/^{86}Sr analysis

Comparison of the ^{87}Sr/^{86}Sr values of duplicates analyzed by solution and LA using both Experiment 1 and 2 techniques reveal that the LA values are elevated relative to solution values, though not by a consistent magnitude (Fig. 3). The hypothesis that LA ratios are not equal to ^{87}Sr/^{86}Sr ratios measured by solution for either experiment is validated by *p*-values indicating strong evidence (Table 7, Experiment 1 p-value = 6.0×10^{-13} and Experiment 2 p-value = 4.5×10^{-12}). To investigate why LA values were offset from solution, we subtracted solution-mode from LA ^{87}Sr/^{86}Sr values of individual conodont duplicates (Δ^{87}Sr/^{86}Sr, Fig. 3). The average Δ^{87}Sr/^{86}Sr with the MC-ICP-MS set at low resolving power and increased plasma sampling depth (torch out, Experiment 1) is 0.000281 (n = 40), greater than the analytical variability defined analyzing the bioapatite iRM GSFR with the same technique (0.000132, n = 35, 2σ). Experiment 2 (medium mass resolving power, torch in) resulted in a lower average Δ^{87}Sr/^{86}Sr (0.000167, n = 73) and closer to the analytical variability obtained analyzing the GSFR in-house iRM with the same technique (0.000155, n = 27, 2σ). This suggests that increased resolving power of the MC-ICP-MS may be more effective at decreasing analytical artifacts than increasing the plasma sampling depth (Fig. 3). Indeed, individual LA ratios measured using increased mass resolving power (Experiment 2) are significantly closer to paired solution ratios (lower Δ^{87}Sr/^{86}Sr; Table 7, p-value: 5.9×10^{-5}) than LA ratios measured using increased sample depth (Experiment 1).

LA analysis yielded less precise values than solution analysis of conodonts for ^{87}Sr/^{86}Sr. LA analysis for both experiments, with a mean

two-standard-error (2SE) of 0.000082 (n = 113), is less likely to provide the true population mean than solution analysis, which in this study had a mean 2SE of 0.000010 (n = 28). Comparison of the two LA experiments reveals that the increased mass resolving power of Experiment 2 (mean 2SE: 0.000072, n = 73) did result in an order of magnitude lower standard error relative to Experiment 1 (mean 2SE: 0.000101, n = 40). Hypothesis testing supports the conclusion that ^{87}Sr/^{86}Sr values derived using the Experiment 2 set up are more precise than values from Experiment 1 (Table 7). While increased mass resolution (Experiment 2) yields more precise values than increased sampling depth (Experiment 1), the potential analytical precision that can be obtained for LA ^{87}Sr/^{86}Sr analysis is further compromised by the consistent elevation of LA over solution values.

The source of the offset between LA and solution ^{87}Sr/^{86}Sr values was investigated by comparison of conodont characteristics with Δ^{87}Sr/^{86}Sr. Albid tissue exhibits a Δ^{87}Sr/^{86}Sr smaller than that of hyaline tissues for both experiments (Fig. 3). The hypothesis that the average Δ^{87}Sr/^{86}Sr for hyaline tissues is larger than the Δ^{87}Sr/^{86}Sr for albid tissues is not validated using a *t*-test (Table 7). Construction of a robust dataset for testing the conodont tissues with both experiments was not possible due to the limited amount of albid tissue. The dataset did not reveal a correlation between Δ^{87}Sr/^{86}Sr and conodont CAI or host-rock lithology.

3.2. Evaluation of spectral interferences

The variable magnitude elevation of LA values relative to solution ^{87}Sr/^{86}Sr values, found in both experiments (Fig. 3), led us to evaluate whether ^{87}Rb, doubly charged REEs (Er, Yb), and molecular complexes (FeP) were interfering on the masses of Sr (Table 1) even after applying common data reduction techniques. We measured the conodonts for ^{166}Er and ^{172}Yb as a proxy for the interfering doubly charged REEs using LA quadrupole ICP-MS. We also measured ^{57}Fe concentrations because we suspected ^{56}Fe^{31}P$^+$ could cause the elevated ^{87}Sr/^{86}Sr values of Experiment 2, which used a resolving power high enough (~7500) to screen out CaPO$^+$, ArPO$^+$, Yb^{2+}, and Er^{2+}, but not FeP$^+$ (compare masses from Table 1).

Conodont Rb/Sr, Er/Sr, Yb/Sr, and Fe/Sr exhibit variation (Fig. 4) comparable to that of previously analyzed conodonts (Trotter and
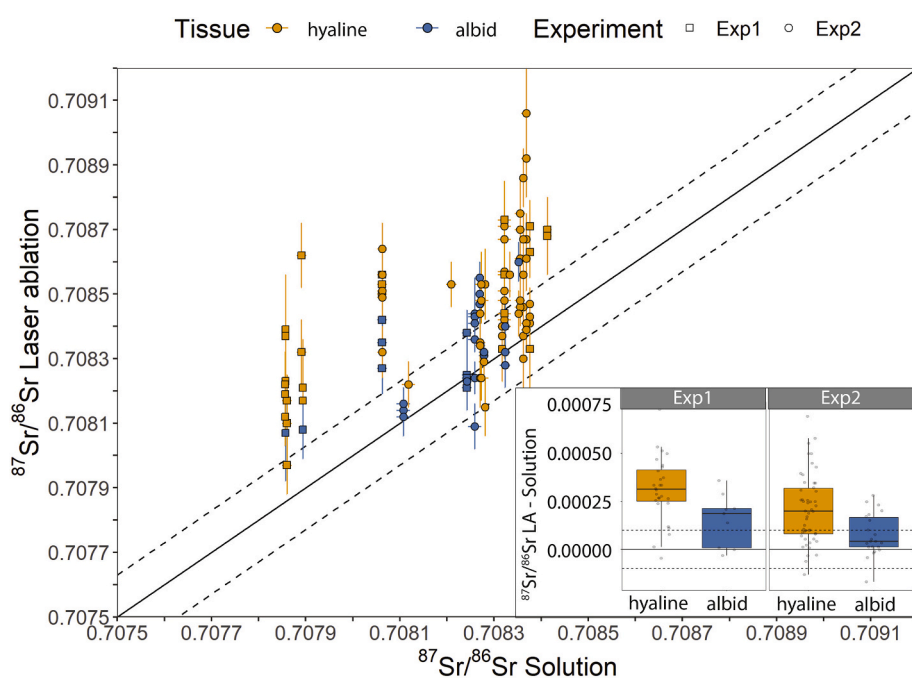

Fig. 3. Measured conodont ^{87}Sr/^{86}Sr analyzed by solution and LA MC-ICP-MS modes. For LA analysis, squares are values measured in low-resolution mode with the torch backed away from the source (Experiment 1) while circles are values measured in with medium mass resolution and the torch at a normal position (Experiment 2). X- and y-error bars are 2SE. Hyaline tissues are orange and albid tissues are blue. Solid black line is the 1:1 line. The standard precision of individual analyses (±2SE) are illustrated by the dashed lines, and defined by measurement of NIST SRM 987 for solution (0.000004, n = 44) and an internal bioapatite reference material, GSFR, for LA (0.000013, n = 62). Bottom right inset contains box plots of LA ^{87}Sr/^{86}Sr minus solution ^{87}Sr/^{86}Sr values (Δ^{87}Sr/^{86}Sr) for each tissue type and experiment. Dashed lines in inset window are 2SE of GSFR measured by LA MC-ICP-MS (0.000013, n = 62). (For interpretation of the references to colour in this figure legend, the reader is referred to the web version of this article.)
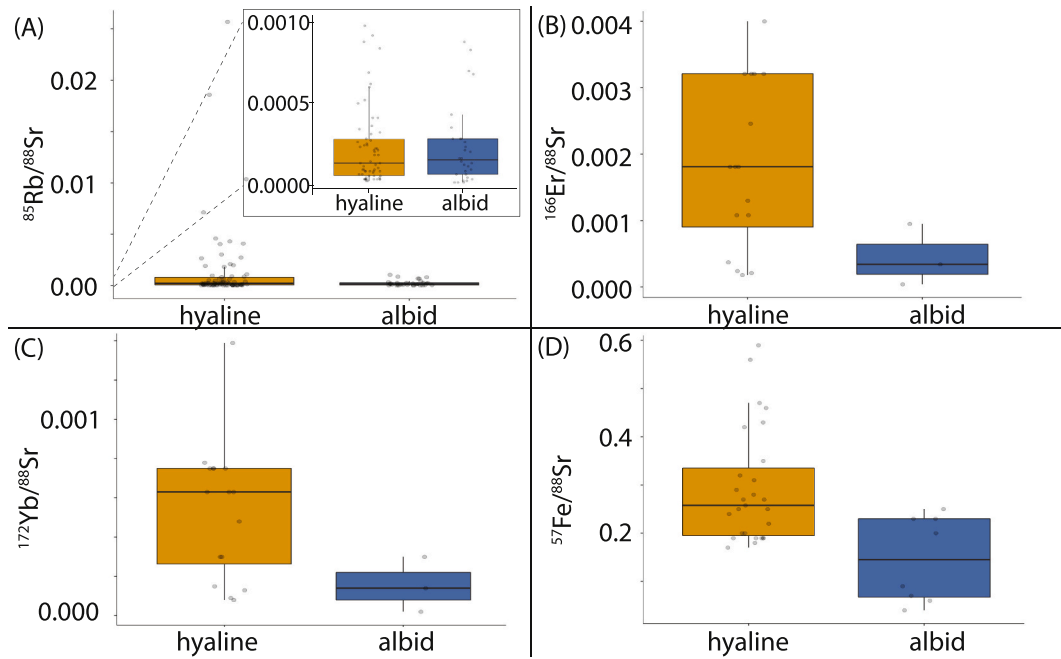
Fig. 4. Box plots of trace elements within individual conodonts with hyaline in orange and albid tissue in blue. (A) $^{85}Rb/^{88}Sr$ measured by LA MC-ICP-MS ($n = 113$). Note inset plot showing distribution between 0.000 and 0.001 $^{85}Rb/^{88}Sr$ ($n = 42$). (B) $^{166}Er/^{88}Sr$ measured by LA ICP-MS ($n = 21$). (C) $^{172}Yb/^{88}Sr$ measured by LA ICP-MS (n = 21). (D) $^{57}Fe/^{88}Sr$ measured by LA ICP-MS ($n = 35$). (For interpretation of the references to colour in this figure legend, the reader is referred to the web version of this article.)

Eggins, 2006). Hyaline tissue of conodonts on average contain higher ratios of Rb/Sr, Fe/Sr, and Er/Sr (respectively 0.0014, 0.2940, 0.0018) in comparison with albid tissues (respectively 0.0003, 0.1463, 0.0017). Yb/Ca was higher in albid tissue (0.0008) than in hyaline (0.0005). We found no significant correlation between $\Delta^{87}Sr/^{86}Sr$ and Er/Sr, Yb/Sr, and Fe/Sr (Table 8), indicating that doubly-charged REEs and FeP$^+$ are not responsible for the elevated conodont $^{87}Sr/^{86}Sr$ ratios measured by LA MC-ICP-MS. Only Rb/Sr presents a statistically significant correlation with $\Delta^{87}Sr/^{86}Sr$ (Table 8) and thus could be responsible for the elevation of LA over solution measurements.

3.3. Intra-sample variability

Comparison of measured $^{87}Sr/^{86}Sr$ values of duplicates, or conodonts extracted from the same stratigraphic interval, indicates variability within samples. In order to investigate variability within a stratigraphic interval, we calculated the uncertainty of the mean for duplicate analyses (McArthur et al., 2001). The uncertainty of the mean for five solution MC-ICP-MS duplicates, comprised of one to 16 conodonts each, from the stratigraphic level 93-RS-77-IG is 0.000020, which is an order of magnitude larger than the two-standard-deviation for NIST SRM 987
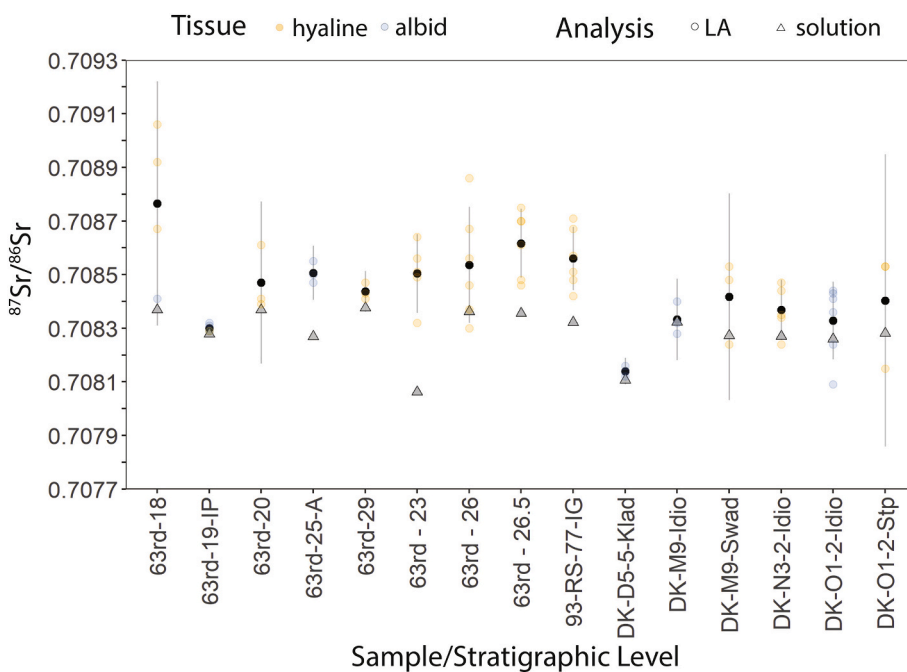

Fig. 5. Plot illustrating conodont $^{87}Sr/^{86}Sr$ variability within an individual sample or stratigraphic interval. Black circles are mean laser ablation MC-ICP-MS $^{87}Sr/^{86}Sr$ value for that stratigraphic interval and black error bars are the uncertainty of the mean. Orange and blue circles are individual LA MC-ICP-MS $^{87}Sr/^{86}Sr$ values for hyaline and albid tissues, respectively. Triangles are solution MC-ICP-MS $^{87}Sr/^{86}Sr$ values and errors bars are encompassed within size of symbol. (For interpretation of the references to colour in this figure legend, the reader is referred to the web version of this article.)

(0.000008, $n = 44$). For LA analysis, we compared duplicate measurements made in medium mass resolution mode with the torch in (Experiment 2) from 15 different stratigraphic intervals ($n = 3$ to 9 conodonts) and calculate uncertainty of the mean with a 95% confidence interval for each level (Fig. 5). The average 95% confidence interval around the mean for each of these stratigraphic levels (0.000197, $n = 15$) is greater than the uncertainty of the mean for the bioapatite GSFR iRM analyzed using Experiment 2 conditions, 0.000155 ($n = 27$). Albid tissues tend to yield lower uncertainty and averages closer to solution values than hyaline tissues (Fig. 5). The fact that duplicate analyses made using solution and laser ablation techniques both exhibit more uncertainty than reference materials suggests that conodonts from the same stratigraphic interval exhibit a range of $^{87}Sr/^{86}Sr$ values greater than analytical precision, irrespective of tissue type.

4. Discussion

Increased mass resolution (Experiment 2) produces more accurate and precise conodont $^{87}Sr/^{86}Sr$ values by LA MC-ICP-MS than increasing the torch distance (Experiment 1). Configuring the MC-ICP-MS with higher mass resolving power reduces spectral interferences ($CaPO^+/ArPO^+$, Yb^{2+}, Er^{2+}) on the masses of Sr, resulting in LA conodont $^{87}Sr/^{86}Sr$ values that are closer to those measured by solution analysis of the same samples (Fig. 3, Table 7). The reduction in interferences with increased mass resolution also improves precision of LA conodont $^{87}Sr/^{86}Sr$ values, as indicated by the reduced standard error of Experiment 2 values in comparison to values from Experiment 1 (Table 7).

Laser ablation analyses of albid tissue produce more accurate $^{87}Sr/^{86}Sr$ values than hyaline tissue (Fig. 3) because of differences in histology. TEM imaging of albid and hyaline tissues of conodonts demonstrates that hyaline tissues exhibit higher porosity, higher permeability, and smaller apatite crystal size in comparison with albid tissue (Trotter et al., 2007). Due to these differences, hyaline tissues likely experienced more recrystallization post-mortem and incorporated larger amounts of Rb, Fe, and REEs (Tütken et al., 2008) that create isobaric interferences on the masses of Sr used to calculate $^{87}Sr/^{86}Sr$ ratios. These elements are more abundant in hyaline tissue relative to albid tissue (Fig. 4), which is why hyaline tissue LA $^{87}Sr/^{86}Sr$ values are more offset from solution than albid tissue LA $^{87}Sr/^{86}Sr$ values (Fig. 3). Increased mass resolution reduces some of these isobaric interferences, which is why $\Delta^{87}Sr/^{86}Sr$ (difference between laser and solution) is lower for both tissues in Experiment 2 relative to Experiment 1 (Fig. 3).

Our experiments suggest that a multitude of spectral interferences could be responsible for the elevation of LA $^{87}Sr/^{86}Sr$ values relative to solution values. Rubidium is a statistically significant interference (Table 8), suggesting that the Rb correction is insufficient. This could be due to the assumptions made for the ^{87}Rb correction: using natural abundance of $^{85}Rb/^{87}Rb$ and the Sr mass bias function to estimate the ^{87}Rb signal (Jackson and Hart, 2006; Vroon et al., 2008; Zhang et al., 2018). Using sample-standard bracketing with matrix-matched materials of known $^{87}Sr/^{86}Sr$ to determine more accurate Rb corrections (Jackson and Hart, 2006; Vroon et al., 2008; Zhang et al., 2018), however, was not possible in this study due to the lack of a matrix appropriate (fossil bioapatite) homogenous reference materials. Based on previous studies applying Rb corrections at higher Rb/Sr concentrations in various minerals (Ramos et al., 2004; Horstwood et al., 2008), we removed all conodonts analyzed in Experiment 2 with $^{85}Rb/^{88}Sr$ larger than 0.001 ($n = 15$) to address the Rb interference. Of the remaining LA analyses, all LA values are within two-standard-deviation of the solution values produced from the same stratigraphic level, but 90% are elevated relative to solution $^{87}Sr/^{86}Sr$ values. The failure of the correction to fully reduce the $\Delta^{87}Sr/^{86}Sr$ to solution value suggests that Rb is not the sole isobaric interference creating the offset. We postulate that the FeP^+ molecular interference may also be playing a part as the mass resolving power required to separate $^{56}Fe^{31}P^+$ from ^{87}Sr is larger than available on current systems (see Table 1 and Eq. (1)). While no statistical correlation

between conodont Fe/Sr and $\Delta^{87}Sr/^{86}Sr$ was significant, this could be a consequence of the small sample size of this dataset and the limited space for ablation on individual conodonts (0.063 to 2 mm).

Analysis of the results of our experiments indicates that the optimal technique for LA MC-ICP-MS analysis of conodonts for $^{87}Sr/^{86}Sr$ is to ablate albid tissue with $^{85}Rb/^{88}Sr$ concentrations lower than 0.001 using enhanced mass resolving power (Experiment 2). The average $\Delta^{87}Sr/^{86}Sr$ for conodonts with albid tissue and low Rb ($^{85}Rb/^{88}Sr < 0.001$) is 0.000080 ($n = 21$), well within the analytical precision of this technique based on the variability of the GSFR reference material (2SD = 0.000155, Table 4). Given that albid tissues are not present in all conodonts (e.g., Trotter et al., 2007) future studies realistically will also need to analyze hyaline tissue. LA MC-ICP-MS of conodonts for $^{87}Sr/^{86}Sr$, regardless of tissue, is viable given that the average $\Delta^{87}Sr/^{86}Sr$ for all (albid and hyaline) Experiment 2 analyses with low Rb ($n = 58$) is 0.000146, still within the analytical precision. Further, the two-standard-deviation uncertainty of all (albid and hyaline) Experiment 2 analyses are within the two-standard-error uncertainty of solution measurements on conodonts from the same stratigraphic level.

The true $^{87}Sr/^{86}Sr$ value of a sample, or one stratigraphic level, is likely more variable than the precision of either LA and/or solution analyses. That intra-sample variability is beyond analytical precision is demonstrated by duplicate solution analyses of conodont aliquots extracted from the same stratigraphic level (sample 93-RS-77-IG, see also McArthur et al., 2001). Laser ablation, with the ability to analyze many individual conodonts from one level, also demonstrates the extent of intra-sample variability with uncertainty of the mean values ranging from 0.000018 to 0.000545 (Fig. 5). Variability within duplicate solution and laser analyses demonstrates geologic influences on intrastratigraphic-level variability in $^{87}Sr/^{86}Sr$. The finding of intra-stratigraphic-level variability is consistent with previous studies comparing in $^{87}Sr/^{86}Sr$ measurements on co-existing belemnites, diagenetically screened carbonate micrite, and conodonts that find differences as great as 0.00029 (Jones et al., 1994; Chen et al., 2018).

Sources of intra-stratigraphic-level variability in $^{87}Sr/^{86}Sr$ include time averaging, variations in water strontium isotope ratio, and differential diagenesis. Modeling and observations reveal that time averaging by compaction and bioturbation averages only 10^2 to 10^3 years of material (Kowalewski et al., 1998, 2018; Olszewski, 2004), which is less than the ocean mixing time and thus would not capture much variability in seawater $^{87}Sr/^{86}Sr$. Partially restricted basins filled with a mixture of run-off and open ocean seawater may generate regional variability in $^{87}Sr/^{86}Sr$, as seen in conodont $^{87}Sr/^{86}Sr$ records from the Carboniferous-age Donets Basin, Ukraine (Montañez et al., 2018). This is not the only mechanism, however, as intra-level variability in conodont $^{87}Sr/^{86}Sr$ is found in a variety of depositional environments (Table 2, Fig. 5). What is most likely is that intra-stratigraphic-level variability in conodont $^{87}Sr/^{86}Sr$ results from differential diagenesis of conodonts caused by exchange of bioapatite strontium with pore waters (Martin and Scher, 2004) or phyllosilicates (Saltzman et al., 2014). Whatever the cause, heterogeneity within individual stratigraphic levels means that the precision of solution $^{87}Sr/^{86}Sr$ measurements averaging several conodonts is not representative of the geologic variability in $^{87}Sr/^{86}Sr$. As such, the reduced sample size required for LA MC-ICP-MS analysis of conodonts for $^{87}Sr/^{86}Sr$ is tremendously valuable. Analysis of smaller sample sizes enables identification of this variability that may be due to, and thus record geologic processes. The rapidity of laser analysis enables larger datasets with better counting statistics to more accurately identify strontium isotopic composition.

The inability to constrain conodont $^{87}Sr/^{86}Sr$ values for individual stratigraphic levels translates to a lack of precision in age estimates made by matching fossil to the seawater $^{87}Sr/^{86}Sr$ curve. The precision of a conodont $^{87}Sr/^{86}Sr$ value within a stratigraphic height can be converted to a number of years by using the slope of the seawater $^{87}Sr/^{86}Sr$ curve. Division of the rate of change (d($^{87}Sr/^{86}Sr$)/dt) of the seawater $^{87}Sr/^{86}Sr$ curve by the analytical precision ($\pm^{87}Sr/^{86}Sr$) yields the

number of years over which that range of $^{87}Sr/^{86}Sr$ values is possible. Age precision calculated this way varies depending upon geologic period, as the rate of change of the seawater $^{87}Sr/^{86}Sr$ curve varies through time (McArthur et al., 2001). We calculated an age precision for this study, which utilizes conodonts extracted from rocks deposited between 346 and 304 Ma (Table 2). The average of the absolute value of the rate of change in $^{87}Sr/^{86}Sr$ for this Carboniferous window is 0.000026/Ma (see Fig. 2B of McArthur et al., 2001), indicating that between 346 and 304 Ma, the average rate of increase or decrease in seawater $^{87}Sr/^{86}Sr$ was 0.000026 per every 1 million years. The average rate of change was then divided by the average uncertainty of the mean for LA analyses (0.000093) measured under ideal conditions (Exp 2 configuration, albid tissue, $^{85}Rb/^{88}Sr < 0.001$). The result is an age uncertainty of ~3.6 Myr for one stratigraphic level when determined by conodont $^{87}Sr/^{86}Sr$ using LA MC-ICP-MS. Note that this age uncertainty is specific the mid-Carboniferous, and the age offset will vary through time depending upon the rate of change of the seawater $^{87}Sr/^{86}Sr$ curve and the inflection of the $^{87}Sr/^{86}Sr$ seawater curve at the time of mineralization.

5. Conclusions

Laser ablation MC-ICP-MS for determining $^{87}Sr/^{86}Sr$ of conodont bioapatite using albid material with low Rb ($^{85}Rb/^{88}Sr < 0.001$) and the instrument configured with enhanced mass resolving power ($m/\Delta m = $ ~7500) was found to be five times the precision and offset an average of 0.000080 relative to traditional solution methods. The offset relates to bioapatite spectral interferences which are eliminated by solution methods that purify Sr and attenuate the sample matrix. Further, variable conodont trace element concentrations generate spatially irregular interferences that preclude an off-line correction of the $^{87}Sr/^{86}Sr$ offset between LA and solution values. LA $^{87}Sr/^{86}Sr$ values produced by this technique are within two-standard-deviation of solution values. However, calculations of the uncertainty of the mean for a stratigraphic interval based on LA MC-ICP-MS analyses of individual conodonts reveals variability in $^{87}Sr/^{86}Sr$ beyond analytical precision. This finding indicates geologic variability in $^{87}Sr/^{86}Sr$ larger than analytical precision and not captures by solution $^{87}Sr/^{86}Sr$ analyses that homogenize multiple conodonts. The geologic variability decreases the precision of ages derived from strontium isotope chronostratigraphy. LA analysis offers a technique for rapid, high-resolution measurements of conodont $^{87}Sr/^{86}Sr$ as well as the ability to investigate intra-stratigraphic-level $^{87}Sr/^{86}Sr$ variability, revealing geologic variability in $^{87}Sr/^{86}Sr$ of interest for chemostratigraphic studies.

Declaration of Competing Interest

The authors declare that they have no known competing financial interests or personal relationships that could have appeared to influence the work reported in this paper.

Acknowledgements

References

Banner, J.L., 2004. Radiogenic isotopes: systematics and applications to earth surface processes and chemical stratigraphy. Earth Sci. Rev. 65 (3–4), 141–194.

Barham, M., Joachimski, M.M., Murray, J., Williams, D.M., 2012. Diagenetic alteration of the structure and $\delta^{18}O$ signature of Palaeozoic fish and conodont apatite: potential use for corrected isotope signatures in palaeoenvironmental interpretation. Chem. Geol. 298-299, 11–19.

Benson, A., Kinsley, L., Willmes, M., Defleur, A., Kokkonen, H., Mussi, M., Grün, R., 2013. Laser ablation depth profiling of U-series and Sr isotopes in human fossils. J. Archeol. Sci. 40, 2991–3100. https://doi.org/10.1016/j.jas.2013.02.028.

Berna, F., Matthews, A., Weiner, S., 2004. Solubilities of bone mineral from archaeological sites: the recrystallization window. J. Archael. Sci. 31 (7), 867–882.

Bizzarro, M., Simonetti, A., Stevenson, R.K., Kurszlaukis, S., 2003. $^{87}Sr/^{86}Sr$ investigation of igneous apatites and carbonates using laser-ablation MC-ICP-MS. Geochim. Cosmochim. Acta 67 (2), 289–302.

Brand, U., Bruckschen, P., 2002. Correlation of the Askyn River section, Southern Urals, Russia, with the Mid-Carboniferous Boundary GSSP, Bird Spring Formation, Arrow Canyon, Nevada, USA: implications for global paleoceanography. Palaeogeogr. Palaeoclimatol. Palaeoecol. 184, 177–193.

Brand, U., Tazawa, J., Hiroyoshi, S., Azmy, K., Lee, X., 2009. Is mid-late Paleozoic Ocean-water chemistry coupled with epeiric seawater isotope records? Geology 37, 823–826.

Chen, J., Montañez, I.P., Qi, Y., Shen, S., Wang, X., 2018. Strontium and carbon isotopic evidence for decoupling of pCO_2 from continental weathering at the apex of the late Paleozoic glaciation. Geology 46 (5), 395–398. https://doi.org/10.1130/G40093.1.

Christensen, J.N., Halliday, A.N., Lee, D.-C., Hall, C.M., 1995. In situ Sr isotopic analysis by laser ablation. Earth Planet. Sci. Lett. 136, 79–85.

Cohen, K.M., Finney, S.C., Gibbard, P.L., Fan, J.-X., 2013. Updated 2020. The ICS international chronostratigraphic chart. Episodes 36, 199–204.

Copeland, S.R., Sponheimer, M., Le Roux, P.J., Grimes, V., Lee-Thorp, J.A., de Ruiter, D. J., Richards, M.P., 2008. Strontium isotope ratios (87Sr/86Sr) of tooth enamel: a comparison of solution and laser ablation multicollector inductively coupled plasma mass spectrometry methods. Rapid Commun. Mass Spectrom. 22, 3187–3194.

Eaton, J.W., Bateman, D., Hauberg, S., Wehbring, R., 2018. GNU Octave Version 4.4.1 Manual: A High-Level Interactive Language for Numerical Computations. URL. https://www.gnu.org/software/octave/doc/v4.4.1/.

Ebneth, S., Diener, A., Buhl, D., Veizer, J., 1997. Strontium isotope systematics of conodonts: Middle Devonian Eifel Mountains, Germany. Palaeogeogr. Palaeoclimatol. Palaeoecol. 132, 79–96.

Epstein, A.G., Epstein, J.D., Harris, L.D., 1977. Conodont Color Alteration – an Index to Organic Metamorphism. USGS Professional Paper 995.

Herwartz, D., Tütken, T., Jochum, K.P., Sander, P.M., 2013. Rare earth element systematics of fossil bone revealed by LA-ICPMS analysis. Geochim. Cosmochim. Acta 103, 161–183.

Horstwood, M.S.A., Evans, J.A., Montgomery, J., 2008. Determination of Sr isotopes in calcium phosphates using laser ablation inductively coupled plasma mass spectrometry and their application to archaeological tooth enamel. Geochim. Cosmochim. Acta 72 (23), 5659–5674.

Irrgeher, J., Galler, P., Prohaska, T., 2016. $^{87}Sr/^{86}Sr$ isotope ratio measurements by laser ablation multicollector inductively coupled plasma mass spectrometry: Reconsidering matrix interferences in bioapatites and biogenic carbonates. Spectrochim. Acta B At. Spectrosc. 125, 31–42.

Jackson, M.G., Hart, S.R., 2006. Strontium isotopes in melt inclusions from Samoan basalts: Implications for heterogeneity in the Samoan plume. Earth Planet. Sci. Lett. 245, 260–270.

Jochum, K.P., Nohl, U., Herwig, K., Lammel, E., Stoll, B., Hofmann, A.W., 2005. GeoReM: a new geochemical database for reference materials and isotopic standards. Geostand. Geoanal. Res. 29 (3), 333–338.

Jochum, K.P., Weis, U., Stoll, B., Kuzmin, D., Yang, Q., Raczek, I., Jacob, D.E., Stracke, A., Birbaum, K., Frick, D.A., Günther, D., Enzweiler, J., 2011. Determination of reference values for NIST SRM 610-617 glasses following ISO guidelines. Geostand. Geoanal. Res. 35 (4), 397–429.

John, E.H., Cliff, R., Wignall, P.B., 2008. A positive trend in seawater $^{87}Sr/^{86}Sr$ values over the Early–Middle Frasnian boundary (Late Devonian) recorded in well-preserved conodont elements from the Holy Cross Mountains, Poland. Palaeogeogr. Palaeoclimatol. Palaeoecol. 269 (3–4), 166–175.

Jones, C.E., Jenkyns, H., 2001. Seawater strontium isotopes, oceanic anoxic events, and seafloor hydrothermal activity in the jurassic and cretaceous. Am. J. Sci. 301, 112–149.

Jones, C.E., Jenkyns, H.C., Hesselbo, S.P., 1994. Strontium isotopes in early Jurassic seawater. Geochim. Cosmochim. Acta 58, 1285–1301.

Keenan, S.W., Engel, A.S., 2017. Early diagenesis and recrystallization of bone. Geochim. Cosmochim. Acta 196, 209–223.

Keenan, S.W., Engel, A.S., Roy, A., Bovenkamp-Langlois, L., 2015. Evaluating the consequences of diagenesis and fossilization on bioapatite lattice structure and composition. Chem. Geol. 413, 18–27.

Kolodny, Y., Luz, B., Sander, M., Clemens, W.A., 1996. Dinosaur bones: fossils or pseudomorphs? The pitfalls of physiology reconstruction from apatitic fossils. Palaeogeogr. Palaeoclimatol. Palaeoecol. 126, 161–171.

Kowalewski, M., Goodfriend, G.A., Flessa, K.W., 1998. High-resolution estimates of temporal mixing within shell beds: the evils and virtues of time-averaging. Paleobiology 24 (3), 287–304.

Kowalewski, M., Casebolt, S., Hua, Q., Whitacre, K.E., Kaufman, D.S., Kosnik, M.A., 2018. One fossil record, multiple time resolutions: disparate time-averaging of echinoids and mollusks on a Holocene carbonate platform. Geology 46 (1), 51–54.

Le Roux, P.J., Lee-Thorp, J.A., Copeland, S.R., Sponheimer, M., de Ruiter, D.J., 2014. Strontium isotope analysis of curved tooth enamel surfaces by laser-ablation multi-collector ICP-MS. Palaeogeogr. Palaeoclimatol. Palaeoecol. 416, 142–149.

Lewis, J., Coath, C.D., Pike, A.W.G., 2014. An improved protocol for ^{87}Sr/^{86}Sr by laser ablation multi-collector inductively coupled plasma mass spectrometry using oxide reduction and a customized plasma interface. Chem. Geol. 390, 173–181.

Martin, E.E., Scher, H.D., 2004. Preservation of seawater Sr and Nd isotopes in fossil fish teeth: bad news and good news. Earth Planet. Sci. Lett. 220 (1–2), 25–39. https://doi.org/10.1016/S0012-821X(04)00030-5.

McArthur, J.M., Howarth, R.J., Bailey, T.R., 2001. Strontium isotope stratigraphy: LOWESS version 3: best fit to the marine Sr-isotope curve for 0-509 Ma and accompanying look-up table for deriving numerical age. J. Geol. 109, 155–170.

Montañez, I.P., Banner, J.L., Osleger, D.A., Borg, L.E., Bosserman, P.J., 1996. Integrated Sr isotope variations and sea-level history of Middle to Upper Cambrian platform carbonates: implications for the evolution of Cambrian seawater ^{87}Sr/^{86}Sr. Geology 24 (10), 917–920.

Montañez, I.P., Osleger, D.A., Banner, J.L., Mack, L.E., Musgrove, M., 2000. Evolution of the Sr and C isotope composition of Cambrian Oceans. GSA Today 10 (5).

Montañez, I.P., Osleger, D.J., Chen, J., Wortham, B.E., Stamm, R.G., Nemyrovska, T.I., Griffin, J.M., Polataev, V.I., Wardlaw, B.R., 2018. Carboniferous climate teleconnections archived in coupled bioapatite δ^{18}O$_{PO4}$ and ^{87}Sr/^{86}Sr records from the epicontinental Donets Basin, Ukraine. Earth Planet. Sci. Lett. 492, 89–101.

Müller, W., Anczkiewicz, R., 2016. Accuracy of laser-ablation (LA)-MC-ICPMS Sr isotope analysis of (bio)apatite – a problem reassessed. J. Anal. At. Spectrom. 31 (1), 259–269.

Munoz, P.M., Alves, A., Azzone, R.G., Cordenons, P., Morano, S., Sproesser, W., de Souza, S., 2016. In situ Sr isotope analyses by LA-MC-ICP-MS of igneous apatite and plagioclase from magmatic rocks at the CPGeo-USP. Br. J. Geol. 46 (Suppl. 1), 227–243.

Olszewski, T.D., 2004. Modeling the influence of taphonomic destruction, reworking, and burial on time-averaging in fossil accumulations. Palaios 19 (1), 39–50.

Patton, C., Hellstrom, J., Paul, B., Woodhead, J., Hergt, J., 2011. Iolite: freeware for the visualization and processing of mass spectrometric data. J. Anal. At. Spectrom. 26, 2508. https://doi.org/10.1039/c1ja10172b.

Prokoph, A., Shields, G.A., Veizer, J., 2008. Compilation and time-series analysis of a marine carbonate d18O, d13C, 87Sr/86Sr and d34S database through Earth history. Earth Sci. Rev. 87, 113–133. https://doi.org/10.1016/j.earscirev.2007.12.003.

R Core Team, 2020. R: A Language and Environment for Statistical Computing. R Foundation for Statistical Computing, Vienna, Austria. URL: https://www.R-project.org/.

Ramos, F.C., Wolff, J.A., Tollstrup, D.L., 2004. Measuring ^{87}Sr/^{86}Sr variations in minerals and groundmass from basalts using LA-MC-ICPMS. Chem. Geol. 211 (1–2), 135–158.

Raymo, M.E., Ruddiman, W.F., 1992. Tectonic forcing of late Cenozoic climate. Nature 359, 117–122.

Reyes, A.V., Carlson, A.E., Beard, B.L., Hatfield, R.G., Stoner, J.S., Winsor, K., Welke, B., Ullman, D.J., 2014. South Greenland ice-sheet collapse during marine isotope stage 11. Nature 510 (7506), 525.

Ruppel, S.C., James, E.W., Barrick, J.E., Nowlan, G.S., Uyeno, T.T., 1996. High-resolution ^{87}Sr/^{86}Sr chemostratigraphy of the Silurian: implications for event correlation and strontium flux. Geology 24 (9), 831–834.

Saltzman, M.R., Edwards, C.T., Leslie, S.A., Dwyer, G.S., Bauer, J.A., Repetski, J.E., Harris, A.G., Bergström, S.M., 2014. Calibration of a conodont apatite-based Ordovician ^{87}Sr/^{86}Sr curve to biostratigraphy and geochronology: implications for stratigraphic resolution. Geol. Soc. Am. Bull. 126 (11–12), 1551–1568.

Sellheim, H., Willmes, M., Hobbs, J.A., Glessner, J.J.G., Jackson, Z.J., Merz, J.E., 2017. Validating fin ray microchemistry as a tool to reconstruct the migratory history of white sturgeon acipenser transmontanus. Trans. Am. Fish. Soc. 146 (5), 844–857. https://doi.org/10.1080/00028487.2017.1320305.

Simonetti, A., Buzon, M.R., Creaser, R.A., 2008. In-situ elemental and Sr isotope investigations of human tooth enamel by laser ablation MC-ICP-MS. Archaeometry 50 (2), 371–385.

Song, H., Wignall, P.B., Tong, J., Song, H., Chen, J., Chu, D., Tian, L., Luo, M., Zong, K., Chen, Y., Lai, X., Zhang, K., Wang, H., 2015. Integrated Sr isotope variations and global environmental changes through the Late Permian to early Late Triassic. Earth Planet. Sci. Lett. 424, 140–147.

Sweet, W.C., Donoghue, P.C.J., 2001. Conodonts: past, present, future. J. Paleontol. 1174–1184. https://doi.org/10.1017/S0022336000017224.

Trauth, M.H., 2010. MATLAB® Recipies for Earth Sciences. Springer Publishing Company, Inc.

Trotter, J.A., Eggins, S.M., 2006. Chemical systematics of conodont apatite determined by laser ablation ICPMS. Chem. Geol. 233 (3–4), 196–216.

Trotter, J.A., Gerald, J.D.F., Kokkonen, H., Barnes, C.R., 2007. New insights into the ultrastructure, permeability, and integrity of conodont apatite determined by transmission electron microscopy. Lethaia 40 (2), 97–110.

Trueman, C.N., Tuross, N., 2002. Trace elements in recent and fossil bone apatite. Rev. Mineral. Geochem. 48 (1), 489–521.

Tuross, N., Behrensmeyer, A.K., Eanes, E.D., 1989. Strontium increases and crystallinity changes in taphanomic and archaeological bone. J. Archaeol. Sci. 16 (6), 661–672.

Tütken, T., Vennemann, T.W., Pfretzschner, H.U., 2008. Early diagenesis of bone and tooth apatite in fluvial and marine settings: constraints from combined oxygen isotope, nitrogen and REE analysis. Palaeogeogr. Palaeoclimatol. Palaeoecol. 266 (3–4), 254–268.

Van Der Meer, D.G., Zeebe, R.E., van Hinsbergen, D.J.J., Sluijs, A., Spakman, W., Torsvik, T.H., 2014. Plate tectonic controls on atmospheric CO2 levels since the Triassic. Proc. Natl. Acad. Sci. 111 (12), 4380–4385.

Vroon, P.Z., van der Wagt, B., Koornneef, J.M., Davies, G.R., 2008. Problems in obtaining precise and accurate Sr isotope analysis from geological materials using laser ablation MC-ICPMS. Anal. Bioanal. Chem. 390 (2), 465–476.

Wenzel, B., Lécuyer, C., Joachimski, M., 2000. Comparing oxygen isotope records of Silurian calcite and phosphate - δ^{18}O compositions of brachiopods and conodonts. Geochim. Cosmochim. Acta 64 (11), 1859–1872.

Wieser, M., Schwieters, J., Douthitt, C., 2012. Multi-collector inductively coupled plasma mass spectrometry. In: Vanhaecke, F., Degryse, P. (Eds.), Isotopic Analysis: Fundamentals and Applications Using ICP-MS. https://doi.org/10.1002/9783527650484.ch3.

Willmes, M., Kinsley, L., Moncel, M.H., Armstrong, R.A., Aubert, M., Eggins, S., Grün, R., 2016a. Improvement of laser ablation in situ micro-analysis to identify diagenetic alteration and measure strontium isotope ratios in fossil human teeth. J. Archaeol. Sci. 70, 102–116.

Willmes, M., Glessner, J.J.G., Carleton, S.A., Gerrity, P.C., Hobbs, J.A., 2016b. ^{87}Sr/^{86}Sr isotope ratio analysis by laser ablation MC-ICP-MS in scales, spines, and fin rays as a nonlethal alternative to otoliths for reconstructing fish life history. Can. J. Fish. Aquat. Sci. 73 (12), 1852–1860.

Willmes, M., Ransom, K.M., Lewis, L.S., Denney, C.T., Glessner, J.J.G., Hobbs, J.A., 2019. IsoFishR: an application for reproducible data reductio and analysis of strontium isotope ratios (^{87}Sr/^{86}Sr) obtained via laser-ablation MC-ICP-MS. PLoS One 13. https://doi.org/10.1371/journal.pone.0204519.

Woodard, S.C., Thomas, D.J., Grossman, E.L., Olszewski, T.D., Yancey, T.E., Miller, B.V., Raymond, A., 2013. Radiogenic isotope composition of Carboniferous seawater from North American epicontinental seas. Palaeogeogr. Palaeoclimatol. Palaeoecol. 370, 51–63.

Woodhead, J., Swearer, S., Hergt, J., Maas, R., 2005. In situ Sr-isotope analysis of carbonates by LA-MC-ICP-MS: interference corrections, high spatial resolution and an example from otolith studies. J. Anal. At. Spectrom. 20 (1), 22.

Woodhead, J., Hellstrom, J., Hergt, J., Greig, A., Maas, R., 2007. Isotopic and elemental imaging of geological materials by laser ablation inductively coupled plasma mass spectrometry. J. Geostandard Geoanal. Res. 31, 331–343.

Wortham, B.E., Wong, C.I., Silva, L.C.R., McGee, D., Montañez, I.P., Rasbury, E.T., Cooper, K.M., Sharp, W.D., Glessner, J.J.G., Santos, R.V., 2017. Assessing response of local moisture conditions in Central Brazil to variability in regional monsoon intensity using speleothem ^{87}Sr/^{86}Sr values. Earth Planet. Sci. Lett. 463, 310–322.

Yang, Y.H., Wu, F.Y., Xie, L.W., Yang, J.H., Zhang, Y.B., 2009. In-situ Sr isotopic measurement of natural geological samples by LA-MC-ICP-MS. Acta Petrol. Sin. 25 (12), 3431–3441.

Yang, Y.H., Wu, F.Y., Xie, L.W., Chu, Z.Y., Yang, J.H., 2014. Re-evaluation of interferences of doubly charged ions of heavy rare earth elements on Sr isotopic analysis using multi-collector inductively coupled plasma mass spectrometry. Spectrochim. Acta B At. Spectrosc. 97, 118–123.

Zhang, L., Ren, W., Wu, Y., Li, N., 2018. Strontium isotope measurement of basaltic glasses by laser ablation multiple collector inductively coupled plasma mass spectrometery based on a linear relationship between analytical bias and Rb/Sr ratios. Rapid Commun. Mass Spectrom. 32, 105–112. https://doi.org/10.1002/rcm.8011.